Received: 3 July 2023 | Revised: 17 December 2023 | Accepted: 3 January 2024

DOI: 10.1002/mp.16942

RESEARCH ARTICLE

MEDICAL PHYSICS

A preliminary study of multispectral Cherenkov imaging and a Fricke-xylenol orange gel film (MCIFF) for online, absolute dose measurement

Haonan Han[1] | **Changran Geng**[1,2,3] | **Xinping Deng**[1] | **Jun Li**[4] | **Diyun Shu**[1,3] | **Xiaobin Tang**[1,2,3]

[1]Department of Nuclear Science and Technology, Nanjing University of Aeronautics and Astronautics, Nanjing, People's Republic of China

[2]Key Laboratory of Nuclear Technology Application and Radiation Protection in Astronautic, Nanjing University of Aeronautics and Astronautics, Ministry of Industry and Information Technology, Nanjing, People's Republic of China

[3]Joint International Research Laboratory on Advanced Particle Therapy, Nanjing University of Aeronautics and Astronautics, Nanjing, People's Republic of China

[4]Radiotherapy Center, Subei People's Hospital of Jiangsu Province, Yangzhou, People's Republic of China

Correspondence
Changran Geng and Xiaobin Tang, Department of Nuclear Science and Technology, Nanjing University of Aeronautics and Astronautics, Nanjing 210016, People's Republic of China.
Email: gengchr@nuaa.edu.cn and tangxiaobin@nuaa.edu.cn

Funding information
National Natural Science Foundation of China, Grant/Award Numbers: 12005102, 12075120; Jiangsu Planned Projects for Postdoctoral Research Funds, Grant/Award Number: 2021K078A; Natural Science Foundation of Jiangsu Province, Grant/Award Number: BK20220132

Abstract

Background: Cherenkov luminescence imaging has shown potential for relative dose distribution and field verification in radiation therapy. However, to date, limited research utilizing Cherenkov luminescence for absolute dose calibration has been conducted owing to uncertainties arising from camera positioning and tissue surface optical properties.

Purpose: This paper introduces a novel approach to multispectral Cherenkov luminescence imaging combined with Fricke–xylenol orange gel (FXG) film, termed MCIFF, which can enable online full-field absolute dose measurement. By integrating these two approaches, MCIFF allows for calibration of the ratio between two spectral intensities with absorbed dose, thereby enabling absolute dose measurement.

Methods: All experiments are conducted on a Varian Clinac 23EX, utilizing an electron multiplying charge-coupled device (EMCCD) camera and a two-way image splitter for simultaneous capture of two-spectral Cherenkov imaging. In the first part of this study, the absorbance curves of the prepared FXG film, which receives different doses, are measured using a fluorescence spectrophotometer to verify the correlation between absorbance and dose. In the second part, the FXG film is positioned directly under the radiation beam to corroborate the dose measurement capacity of MCIFF across various beams. In the third part, the feasibility of MCIFF is tested in actual radiotherapy settings via a humanoid model, demonstrating its versatility with various radiotherapy materials.

Results: The results of this study indicate that the logarithmic ratios of spectral intensities at wavelengths of 550 ± 50 and 700 ± 100 nm accurately reflect variations in radiation dose ($R^2 > 0.96$) across different radiation beams, particle energies, and dose rates. The slopes of the fitting lines remain consistent under varying beam conditions, with discrepancies of less than 8%. The optical profiles obtained using the MCIFF exhibit a satisfactory level of agreement with the measured results derived from the treatment planning system (TPS) and EBT3 films. Specifically, for photon beams, the lateral distances between the 80% and 20% isodose lines, referred to as the penumbra (P80-20) values, obtained through TPS, EBT3 films, and MCIFF, are determined as 0.537, 0.664, and 0.848 cm, respectively. Similarly, for electron beams, the P80-20 values obtained through TPS, EBT3 films, and MCIFF are found to be 0.432, 0.561, and 0.634 cm, respectively. Furthermore, imaging of the anthropomorphic phantom demonstrates the practical application of MCIFF in real radiotherapy environments.

Conclusion: By combining an FXG film with Cherenkov luminescence imaging, MCIFF can calibrate Cherenkov luminescence to absorbed dose, filling the gap in online 2D absolute dose measurement methods in clinical practice, and providing a new direction for the clinical application of optical imaging to radiation therapy.

KEYWORDS
absolute dose measurement, Cherenkov, Fricke-xylenol orange gel, spectroscopy

1 | INTRODUCTION

The success of radiation therapy greatly depends on accurate dose delivery, which makes dose monitoring a critical aspect.[1,2] At present, TLD and OSLD are frequently employed for point dose measurements in radiotherapy. However, both methods require a readout process, making them unsuitable for online dose monitoring.[3,4] Furthermore, while EPID can facilitate online monitoring of patient positioning and dose, it still encounters challenges related to dose resolution and image artifacts.[5] Currently, no traditional technique can rapidly and easily provide information about the field position and dose distribution; Cherenkov luminescence imaging has garnered significant attention as a highly promising method for implementing online, 2D dose-monitoring applications.[6,7]

Cherenkov radiation refers to the visible light produced within a spectrum of 200–1000 nm when high-velocity charged particles pass through a dielectric medium at velocities surpassing the phase velocity of light in that given medium.[8] The initiation of this radiation stems from the energy loss process undertaken by these charged particles, with a significant correlation existing between the deposited energy and the intensity of the Cherenkov radiation emitted. The unique attributes of Cherenkov radiation make it an ideal candidate for applications to dosimetry-related processes. As a result, Cherenkov radiation dosimetry holds immense promise as a cost-effective and versatile tool for dose monitoring in radiotherapy.[9–11]

Although Cherenkov radiation can effectively monitor beam shape and relative dose distribution in radiotherapy, measuring absolute dose with Cherenkov radiation remains challenging. The primary reasons are the variations in the positions and angles of emission and detection of Cherenkov radiation between different treatment fractions, as well as the significant effects of inherent optical properties such as pigmentation and superficial blood vessels on the absorption and attenuation of Cherenkov lights.[12,13] These factors have the potential to undermine the linear relationship between captured Cherenkov signals and deposited doses, ultimately making it difficult to accurately measure absolute dose through captured Cherenkov light intensity.

Fricke–xylenol orange gel (FXG) dosimeter is widely used as a chemical dosimeter in the field of radiation dosimetry given its reliable and predictable response to absorbed dose.[14] In this dosimeter, the absorbed radiation leads to the oxidation of ferrous ions, which has a conversion yield proportional to the absorbed dose up to saturation.[15] The complex formation between ferric ions and metal ion indicator xylenol orange results in visible-light absorption centered at approximately 550 nm.[16] In this study, a novel method, multispectral Cherenkov luminescence imaging combined with FXG film (MCIFF), for whole-field and online absolute dose measurement is presented. When the Cherenkov light passes through a medium-free environment, the spectrum of the Cherenkov light remains constant, with the number of Cherenkov photons being almost inversely proportional to the wavelength squared. With increasing FXG film absorbed dose, a corresponding increase in its optical absorption near the 550 nm band occurs. Thus, when the Cherenkov light passes through the FXG film, wavelengths around 550 nm are absorbed, leading to alterations in the spectral composition of the Cherenkov light. These changes can be quantified by computing the ratio of Cherenkov light intensities detected within two distinctive wavelength ranges, thereby facilitating the calibration of absorbed dose. The proposed MCIFF is an independent quantitative tool for monitoring dose delivery, that is, not affected by the relative positions of the detector.

2 | METHODS AND MATERIALS

2.1 | Preparation of FXG film

The FXG film is prepared using 4% by weight of gelatin from porcine skin, ultrapure water, 50 mM sulfuric acid (H_2SO_4), 1 mM sodium chloride (NaCl), 1 mM iron sulfate heptahydrate ($FeSO_4{\cdot}7H_2O$), and 0.1 mM xylenol orange ferric ion indicator ($C_{31}H_{28}N_2Na_4O_{13}S$). After preparing the FXG solution, it is transferred to the film molds to prepare FXG films with thicknesses of 3 and 5 mm by controlling the volume of the solution. Upon filling, we cover the containers with lids and place them in the laboratory for approximately 24 h to obtain stable samples that are suitable for experimentation.

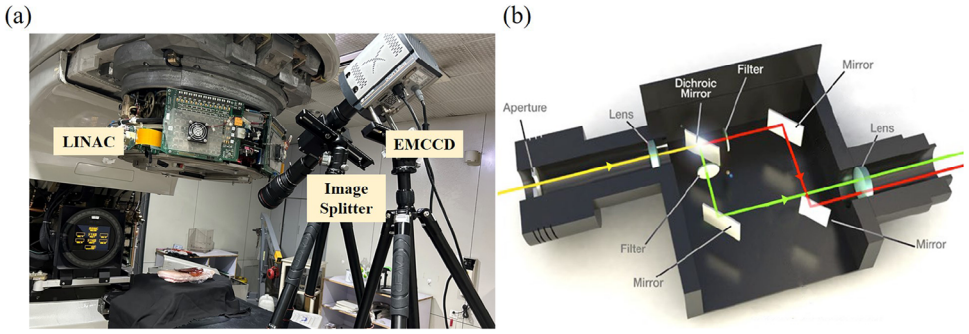

FIGURE 1 (a) Acquisition setup using LINAC for beam delivery and an EMCCD camera with a two-way image splitter for Cherenkov capture. (b) Detailed schematic of the image splitter.

2.2 | Image acquisition and processing

An electron multiplying charge-coupled device (EMCCD) camera (Andor iXon Ultra 888) with a two-way image splitter (Cairn Optosplit II) is used to image the Cherenkov light emitted during radiotherapy over the course of this study. The camera features a 24–70 mm f/2.8L lens (Canon), and its position relative to the LINAC is illustrated in Figure 1a. The camera's sensitivity extends between the wavelengths of 400 and 900 nm. A longpass dichroic beamsplitter with a central wavelength at 600 nm is installed in the image splitter, and two band-pass filters with transmission windows of 550 ± 50 and 700 ± 100 nm are separately installed in corresponding optical paths. The integrated filter cube, as depicted in Figure 1b, enables the beam splitter to segment the image into two independent parts. These two parts can be displayed side by side on a single camera chip, enabling simultaneous view and comparison and providing a significant advantage over manual or electronic filter changers. We determine that an exposure time of 0.5 s is optimal by comparing images captured with different exposure times. A background image with the same exposure time is collected after each beam output and then subtracted from each frame of the images collected during beam output. To eliminate stray radiation-induced noise, we apply a 7 × 7 median filter to each image. To contrast the optical profile with the dose distribution, a characteristic reference point is chosen to align the optical image with the actual object. A scalable factor of 0.032 mm/pixel is established with a calibrated pixel size via the light field approach.[17]

2.3 | Concept of MCIFF for absolute dose measurement

The FXG film prepared in this study exhibits a substantial change in absorbance at two wavelength bands with increasing radiation dose, specifically at 440 and 550 nm. Owing to the radiation-induced oxidation of Fe^{2+} ions to Fe^{3+} ions, the absorbance at 550 nm increases linearly with radiation dose.[15] Conversely, the absorbance at wavelengths above 600 nm is almost independent of the dose. As such, the difference in absorbance between the two wavelength bands is proportional to the dose, that is,

$$A_S - A_L = kD + d, \tag{1}$$

where A_S and A_L are the absorbances of the FXG film at 550 ± 50 and 700 ± 100 nm, corresponding to the short- and long-wavelength bands, respectively. The slope, k, represents the response rate of the prepared FXG dosimeter to the dose, while the intercept, d, represents the difference in absorbance between the two wavelength bands before irradiation. Both k and d are related to the composition of the FXG dosimeter.[18]

According to the definition of absorbance, the absorbances of the FXG film at 550 ± 50 and 700 ± 100 nm, A_S and A_L, respectively, are

$$A_S = log\frac{I_S}{I'_S}, \tag{2}$$

$$A_L = log\frac{I_L}{I'_L}, \tag{3}$$

where I_S and I_L are the Cherenkov light intensities of short- and long-wave lights, respectively, without passing through the FXG film. I_S' and I_L' are the intensities of short- and long-wave lights, respectively, after passing through the FXG film. Through rearrangement, Equation (1) can be expressed as a formula for the relationship between radiation dose and the ratio of light intensities of two bands. We use the logarithm of the ratio of the intensity values at 550 ± 50 and 700 ± 100 nm, L, as a parameter for quantifying the absorbed dose,

$$L = log\frac{I'_L}{I'_S} = kD + log\frac{I_L}{I_S} + d. \tag{4}$$

The Cherenkov light passing through the FXG film can be captured by an EMCCD camera. With an image

splitter located in front of the camera, the Cherenkov light is divided into two spatially equivalent images. After entering the imaging beam splitter through a lens, the light passes through a dichroic mirror with a central wavelength of 600 nm. The light is then divided into two beams based on their respective wavelengths: one with wavelengths less than 600 nm and the other with wavelengths greater than 600 nm. Subsequently, each light passes through a specific bandpass filter (550 $\pm$ 50 and 700 $\pm$ 100 nm) to further narrow down the wavelength range. Finally, both lights are directed to the camera sensor for simultaneous imaging in their respective wavelength ranges, achieved by using a flat mirror for parallel transportation. The logarithmic L has a linear relationship with radiation dose, and the slope of this relationship is related to the FXG film's effect on radiation dose. Through MCIFF, the calibration of Cherenkov light with absorbed dose can be accomplished irrespective of other variables.

2.4 | Experimental radiation delivery

This study is performed on the Clinac 23EX (Varian Medical Systems). To enhance the signal-to-noise ratio of captured images and eliminate the effect of ambient light, all light sources in the treatment room are turned off during the experiment. In the first part of this study, a fluorescence spectrophotometer is used to measure the absorbance curve of the FXG film at varying radiation doses, with the aim of verifying the correlation between absorbance changes and absorbed dose. In the second part, the FXG film is positioned directly under the radiation beam to substantiate the dose measurement capacity of MCIFF in a range of different beams. The third part involves testing the feasibility of MCIFF in actual radiotherapy settings by using a humanoid phantom, demonstrating its wide applicability with different radiotherapy materials. The gantry angle is set to 0°, with a source–skin distance of 100 cm and 2000 monitor units (MU) of dose delivered per beam delivery, unless otherwise indicated. The field size is typically 10 $\times$ 10 cm.

In the first part, experiments are conducted using a photon beam with an energy of 6 MV and a dose rate of 600 MU/min. Ten glass vials containing FXG dosimeters are irradiated with doses ranging from 200 to 2000 MU (in increments of 200 MU). The evaluation technique employed is optical absorption spectrophotometry by using a fluorescence spectrophotometer (1901 PC, Aucy Instrument Co., Ltd.) in the wavelength range from 400 to 800 nm. All optical measurements are performed about 12 h following irradiation. Additionally, x-ray imaging of the prepared FXG films is performed using an x-ray tube with a voltage of 50 kV and a current of 1.6 A, along with a flat panel detector (Pheda1215A, Sensview Co., Ltd.) with a spatial resolution of 100 μm.

The second part validates the application of MCIFF to dose measurements in radiotherapy. An FXG film is prepared and placed horizontally on a couch, and measurements are taken using photon and electron beams with various energies and dose rates. The absolute dose measurement capability of MCIFF is also verified by altering the relative position between the camera and radiation field. The distance between the camera and the field center is 1.8 m, with a 20° angular difference between different positions. Furthermore, the effect of the FXG film with varying thicknesses on the accuracy of dose measurements is investigated.

2.4.1 | Imaging of photon beams

To validate the response of MCIFF to photon beams, a corresponding relationship between L and machine output is examined under various photon beam energies and dose rates. The energy dependence is assessed using photon beams with energies of 6 and 10 MV at a dose rate of 600 MU/min. To investigate its dose rate dependence, experiments are conducted at dose rates of 200, 400, and 600 MU/min. The accuracy and applicability of MCIFF in different treatment environments are evaluated by varying the relative position and angle between the EMCCD camera and the center of the treatment field. The effect of diverse thicknesses of FXG film on dose measurement is investigated by utilizing 3 and 5 mm FXG film exposed to a 6 MV photon beam at 600 MU/min.

2.4.2 | Imaging of electron beams

In electron beams imaging, variations in the beam's dose rate and energy are applied to confirm the dose rate and energy dependency of MCIFF. Two dose rates of 400 and 600 MU/min and two electron energies of 6 and 12 MeV are utilized in experiments.

2.4.3 | Comparison of optical profile and dose distribution

To investigate the measurement accuracy of the proposed method on 2D dose distribution, treatment planning system (TPS) is employed as the gold standard to measure the 2D dose distribution and confirm the consistency between the optical profile and the dose distribution. In addition, an EBT3 film (Ashland Global Holdings Inc.) is also used to assess the 2D relative dose measurement capability of MCIFF. The FXG film is positioned vertically within the treatment field, and the EBT3 film is applied to its surface, situated approximately 2 cm below its upper edge. Photon and electron

beams with energies of 6 MV and 6 MeV are applied at a dose rate of 600 MU/min to deliver a dose of 500 MU.

In the third part of this study, pork is utilized to simulate human tissue because its optical properties are similar to those of human skin and it offers relative uniformity. This similarity allows us to create experimental conditions that closely resemble a real radiotherapy environment. For the measurements on tissue phantoms, the FXG film is positioned horizontally over the pork, and measurements are executed using photon and electron beams with energies of 6 MV and 6 MeV. The dose rate is set to 600 MU/min. To investigate the effect of various radiotherapy materials on dose measurements, the FXG film is placed on bolus, mask samples, and their combination. The bolus has a thickness of 1 cm, while the mask has a thickness of 1 mm. Both the bolus and the mask are authentic radiation therapy materials conventionally utilized in clinical settings. We integrate the measurement results under various radiotherapy conditions into the fitted equation obtained in the second section for dose calculations, and subsequently compared the calculated doses with TPS. These observations are conducted to evaluate the extent of influence exerted by different radiotherapy materials on the quality of dose measurements.

3 | RESULTS

3.1 | Optical characteristics of FXG film

The radiation-induced color changes presented by the FXG film are presented in Figure 2a. The observed color change of the FXG film ranges from orange-yellow (unirradiated) to purple-red (2000 MU). The aforementioned phenomenon is observable under photon and electron irradiation, across a range of particle energies and dose rates. The optical absorption spectra of FXG samples, exposed to doses ranging from 200 to 2000 MU, are depicted in Figure 2c. The x-ray imaging of the FXG films reveals an overall non-uniformity of 3.02% across the entire film area, with no significant differences observed, as depicted is Figure 2b. This demonstrates that the films prepared in this study are sufficiently homogeneous.

The prepared FXG film exhibits two absorption peaks: one at 441 nm corresponding to the initial Fe^{2+} ions in the gel before irradiation and another at 555 nm corresponding to the radiation-induced Fe^{3+}. This study mainly focuses on the changes within the wavelength range of 500–800 nm. As the dose increases, the optical absorption at band 550 ± 50 nm increases, while that at band 700 ± 100 nm remains almost constant. The average absorbance difference between the 550 ± 50 and 700 ± 100 nm bands and the absorbed dose–response curve are shown in Figure 2d. The FXG film shows an excellent linear relationship within the dose range of 0–2000 MU ($R^2 > 0.99$).

3.2 | MCIFF for dose measurements

3.2.1 | Imaging of photon beams

To assess the ability of MCIFF to obtain absolute dose measurements, the average L of six randomly selected regions of interest (ROI) within the radiation field are chosen. Here, L represents the logarithm of the ratio of intensities of the long and short wavelength bands captured by the camera. The measurement uncertainty is evaluated using the standard deviation. Figure 3a presents a schematic diagram of the experiment. In this section, the FXG film is placed directly on the couch to undergo LINAC irradiation. Figure 3b displays the dose–response of L for different photon energies (6 and 10 MV), dose rates (200, 400, and 600 MU/min), and FXG film thicknesses. The slopes, intercepts, and R^2 values for all the fitted lines are presented in Table 1. All the data presented in the figure originate from a single video, with the beam-on and imaging process being continuous throughout. Each dose point corresponds to a specific moment captured in the video. The selection of ROI (60 × 60 pixels) from the central area of the radiation field is shown in Figure 3c. Each line is normalized to 0 at 0 MU to facilitate comparison. Across different photon energies and dose rates, when the thickness of the FXG film is 5 mm, L exhibits an outstanding linear relationship with dose. The slopes are almost identical with a discrepancy below 6%, indicating a minimal effect of photon energy and dose rate in photon radiotherapy on MCIFF. When the FXG film thickness is 3 mm, L also exhibits an excellent linear response to dose, but the slope of the fitting line is significantly different from that at 5 mm thickness under the same photon conditions. The variance between the dose response at different positions and the averaged dose response across multiple positions illustrates the impact of the camera's location on measurement outcomes. As depicted in Figure 3d,e, despite the various relative positions, no significant statistical difference in the response of L exists when tested at a significance level of 0.05 (p = 0.9378, 0.9456, 0.8821).

3.2.2 | Imaging of electron beams

Figure 3f illustrates the correlation between the machine output and L for different electron energies (6 and 12 MeV) and dose rates (400 and 600 MU/min). Across various electron beam conditions, the fitted lines exhibit good linear fits, with deviations from one another being below 8%.

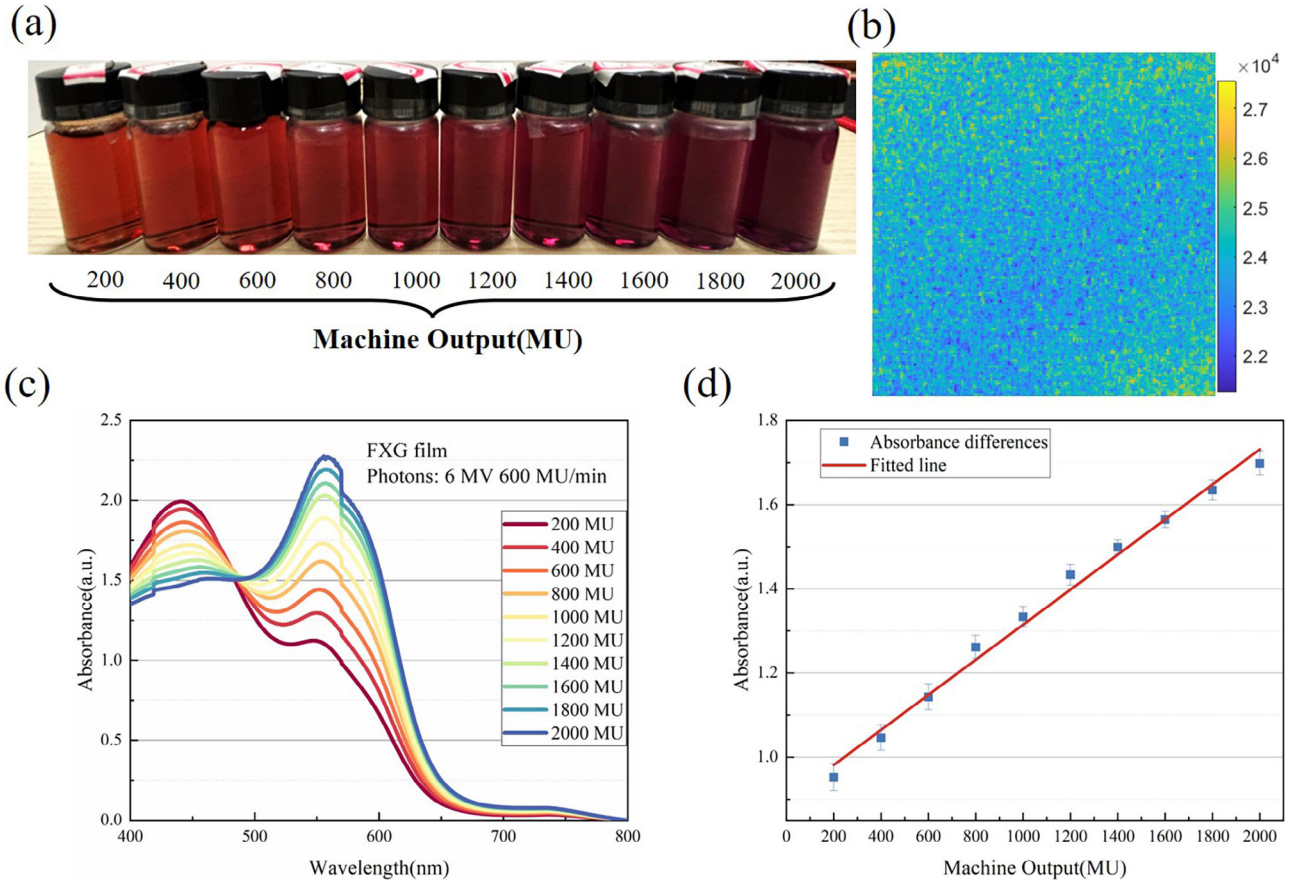

FIGURE 2 (a) Radiation-induced color change presented by the FXG film irradiated with 6 MV photon beam at 600 MU/min. (b) X-ray imaging of the FXG film. (c) Optical absorption spectra of the FXG film within the wavelength range of 400–800 nm. (d) Average absorbance difference between the 550 ± 50 and 700 ± 100 nm bands and dose–response curve of the FXG film.

TABLE 1 The fitting line parameters under different beams and FXG film thickness.

Beam conditions	Slope		Intercept		
	k	Error	*d*	Error	R^2
600 MU/min 5 mm FXG at 6 MV photon	2.882E−4	1.019E−5	−0.366	0.0117	0.9767
600 MU/min 3 mm FXG at 6 MV photon	1.854E−4	6.210E−6	−0.363	0.0071	0.9791
400 MU/min 5 mm FXG at 6 MV photon	2.892E−4	8.368E−6	−0.423	0.0096	0.9843
200 MU/min 5 mm FXG at 6 MV photon	3.052E−4	1.412E−5	−0.338	0.0162	0.9608
600 MU/min 5 mm FXG at 10 MV photon	2.618E−4	1.062E−5	−0.382	0.0122	0.9696
600 MU/min 5 mm FXG at 6 MeV electron	3.123E−4	8.227E−6	−0.349	0.0094	0.9869
400 MU/min 5 mm FXG at 6 MeV electron	3.139E−4	6.134E−6	−0.354	0.0070	0.9927
600 MU/min 5 mm FXG at 12 MeV electron	2.761E−4	6.984E−6	−0.316	0.0080	0.9880

3.2.3 | Comparison of optical profile and dose distribution

The absolute dose distribution obtained from the TPS, in line with the experimental setup, is considered as the gold standard for dose measurements. Subsequently, the irradiated EBT3 film is scanned using a film scanner (Epson V850 Pro). The measured results, *L*, are obtained for each pixel point in the first Cherenkov image, which are considered as the intercepts of the pixel points in Equation (4), $\log\frac{I_L}{I_S} + d$. For the 6 MV photon beam and 6 MeV electron beam, the slopes in Equation (4) are determined from the fitted lines, resulting in values of 2.882×10^{-4} and 3.123×10^{-4}, respectively, as described in the previous section. As *L* is calibrated against machine output in the previous section, when *L* is input into the fitted

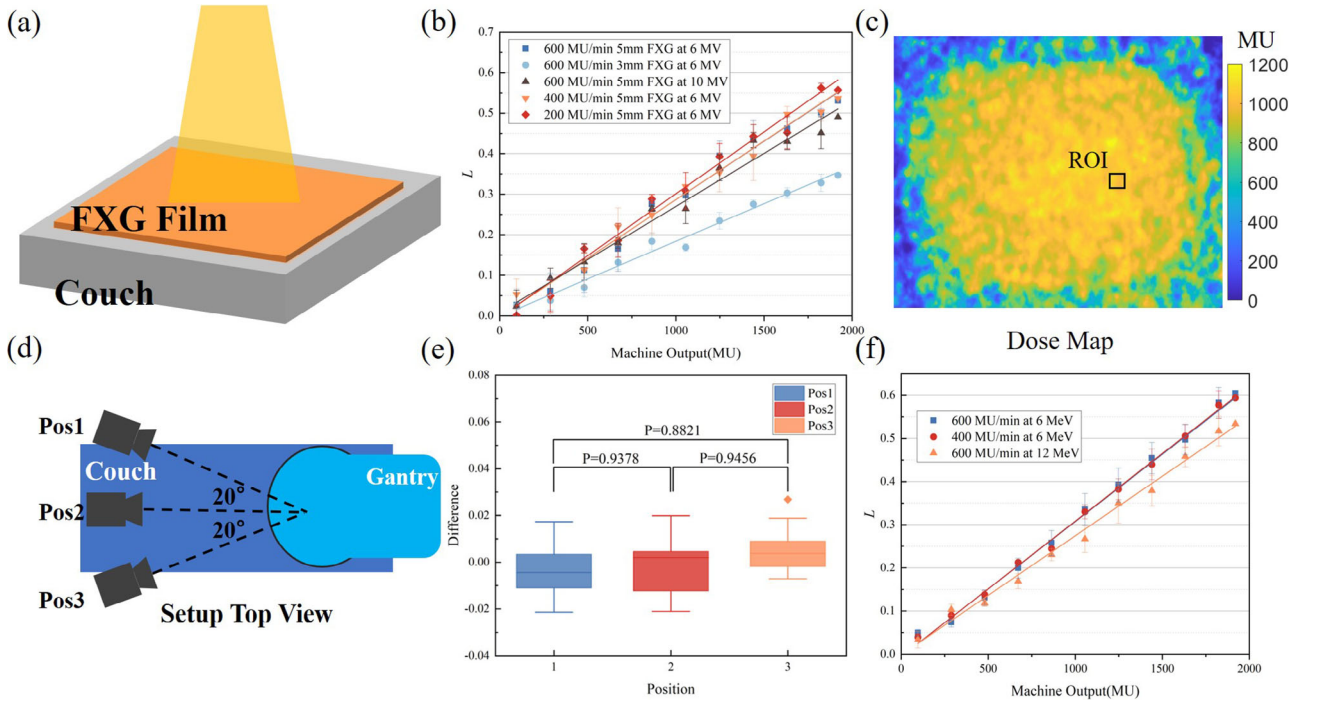

FIGURE 3 (a) Schematic diagram of the experiment. (b) *L* measured under different photon energies (blue, black), dose rates (blue, orange, red), and FXG film thicknesses (blue, light blue) as a function of absorption dose. (c) The calculated distribution of dose when the LINAC outputs 1000 MU. The actual physical size of ROI is 1.92 × 1.92 mm. (d) Top view schematic of the relative positions of the camera and the gantry. (e) Dose–response deviation under different relative positions. The significance of the results is assessed via *t*-test with a significance level of 0.05. (f) Dose–response curves of MCIFF with different electron energies (blue, orange) and dose rates (blue, red).

curve, only the machine output is obtained. To obtain the dose, it is necessary to multiply the machine output by a depth factor. The depth factor is the ratio of the average dose at depths ranging from 0 to 5 mm (thickness of the 5 mm FXG film) to the dose at the maximum dose depth extracted from the TPS, which is 0.79 for photons and 0.83 for electrons. This conversion allows the transformation of *L* into dose. In Figure 4, we compare the relative dose measured by the EBT3 film under photon beams with the absolute dose measured by MCIFF and TPS. The ROI for the lateral dose distribution is located at a depth of 2 cm; for the depth dose distribution, the ROI is positioned at the center of the radiation field from depths ranging between 0 and 10 cm. For each position, three dose points of 60 × 60 pixels are selected within the rectangular ROI and then averaged to determine the dose reading for that particular position. For the photon beam, the penumbra, defined as the lateral distance between the 80% and 20% isodose lines (P80−20), is 0.537, 0.664, and 0.848 cm for the TPS, EBT3 film, and optical measurements, respectively. The dose deviation is determined by subtracting the TPS calculation results from both the optical measurements at each point and the EBT3 film measurement results. The lateral dose differences for photon beams are primarily located at the beam boundary and are less than 14%. Conversely, the depth dose differences are relatively small, amounting to less than 3%. The variation of the FXG film under different dose irradiation is illustrated in Figure 5.

Figure 6 displays a 2D dose comparison between the MCIFF and EBT3 film measurements with the doses obtained from the TPS under electron beams with the same ROI selection as that for photon beams. The MCIFF results under the electron beam show greater consistency with the gold standard TPS results and EBT3 film measurements compared with those under the photon beam, with penumbra of 0.432, 0.561, and 0.634 cm for the TPS, EBT3 film, and MCIFF measurements, respectively. The difference in lateral dose distribution is less than 10%, and the depth dose difference is less than 3%.

3.3 | Imaging on anthropomorphic phantom

In order to simulate a real radiation therapy environment, pork is used as a simulation of human tissue. Radiation therapy materials are placed above it to mimic the actual treatment conditions, and the FXG film is positioned at the top, as shown in Figure 7a,b. The *L* values captured by the camera are incorporated into the fitted curve from the second section for dose measurements. Figure 7c illustrates the ratio between the dose

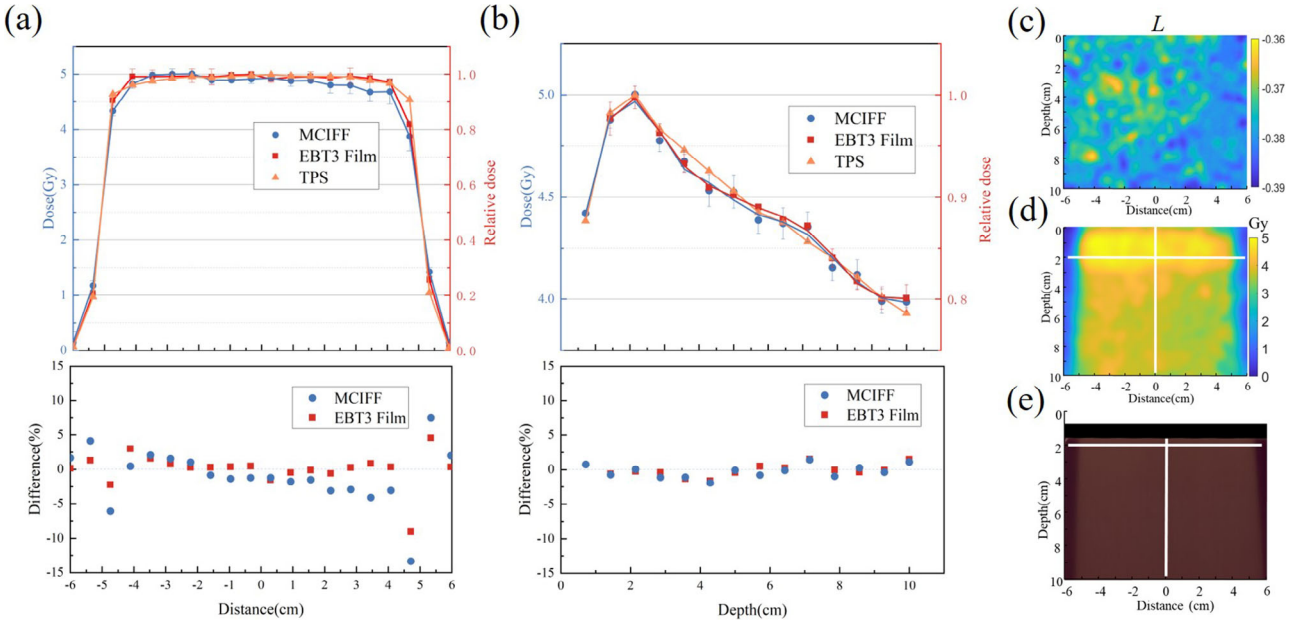

FIGURE 4 Comparison of the MCIFF, EBT3 film, and TPS measurements (top) and the percentage differences between the MCIFF and TPS measurements, as well as between the EBT3 film and TPS measurements (bottom) under photon beams for (a) lateral dose distribution and (b) depth dose distribution. (c) The distribution of *L* in the first Cherenkov light image. (d) 2D measurement results from MCIFF. (e) 2D measurement results from the EBT3 film.

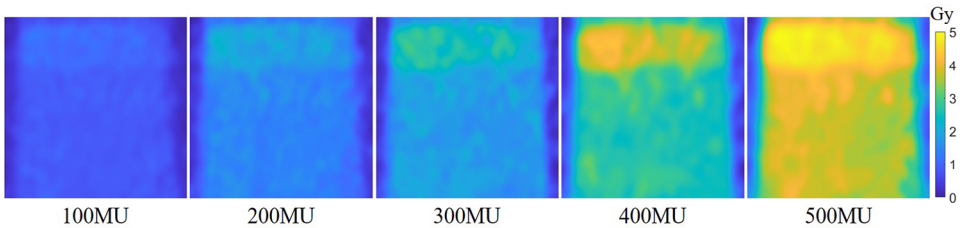

FIGURE 5 The absolute dose distribution measured by MCIFF at different machine outputs.

calculation obtained from the fitting equation and the dose at the 2.5 mm depth (mid-thickness of the FXG film) as per the TPS. The dose calculation method is consistent with Section 3.2.3, where the dose is calculated by first determining *L* as machine output through a fitted curve and then multiplying it by a depth factor to convert it into dose. The selection of ROI is shown in Figure 7d. The difference between the doses measured using MCIFF and the dose from TPS is less than 16%, and as the doses increases, the measurement differences and error bars become progressively smaller.

4 | DISCUSSION

In recent years, significant advancements have occurred on the relative dose distribution and field verification of radiotherapy with Cherenkov imaging.[19,20] In radiotherapy, where precise dose delivery is necessary, measuring only relative dose distribution is insufficient.[21] To utilize Cherenkov imaging for dose measurements, Hachadorian et al. attempted to use x-ray imaging for attenuation correction of Cherenkov light.[22,23] This study proposes an absolute dose measurement method called MCIFF, which combines multispectral Cherenkov luminescence imaging with FXG film. Through the combination of Cherenkov luminescence imaging with FXG film, the ratio of light intensities in two wavebands (550 ± 50 and 700 ± 100 nm) and dose are calibrated based on the distinct absorbance change properties at different wavebands after the FXG film is irradiated.

The changes in absorbance of the FXG film after irradiation, depicted in Figure 2b, align with those found in Gambarini et al.'s prior research.[16] The outcomes suggest that the FXG film fabricated in this study adheres to the criteria and is applicable for use in subsequent experiments. The results in Figure 3a demonstrate an outstanding linear relationship between *L* and absorbed dose, irrespective of the radiation conditions. Moreover, the slopes of the different fitted lines are almost

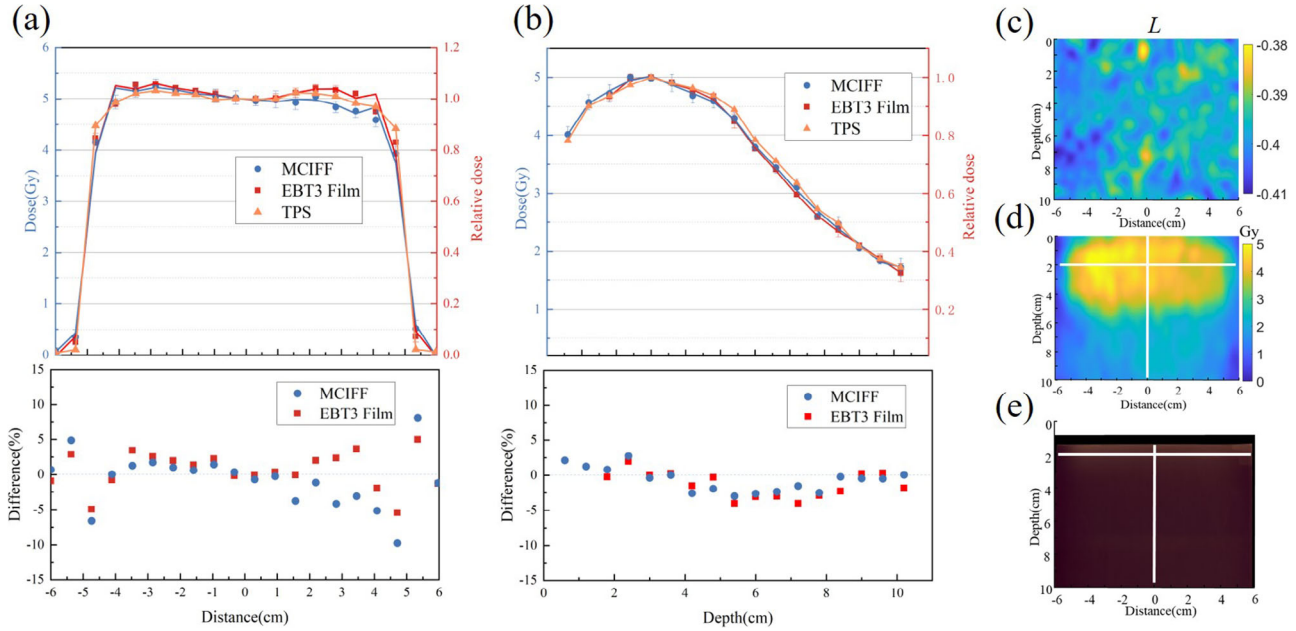

FIGURE 6 Comparison of the MCIFF, EBT3 film, and TPS measurements (top) and the percentage differences between the MCIFF and TPS measurements, as well as between the EBT3 film and TPS measurements (bottom) under electron beams for (a) lateral dose distribution and (b) depth dose distribution. (c) The distribution of *L* in the first Cherenkov light image. (d) 2D measurement results from MCIFF. (e) 2D measurement results from the EBT3 film.

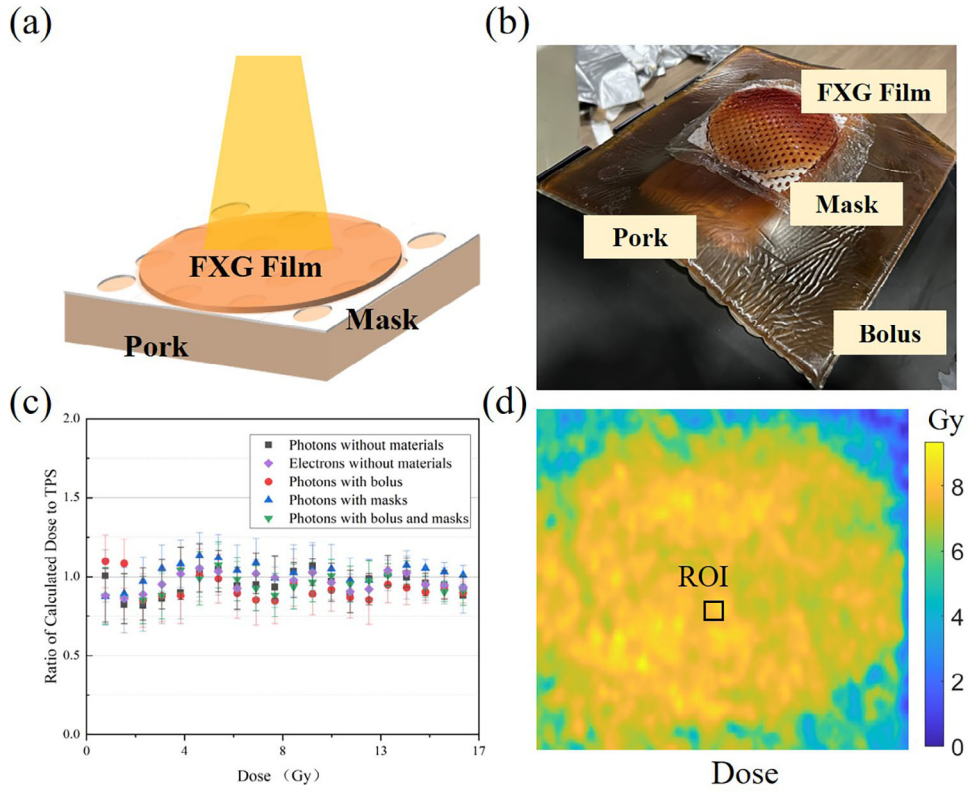

FIGURE 7 The experimental setup schematic (a) and image (b) of combining FXG film and tissue phantom with radiotherapy materials. (c) The ratio of MCIFF dose measurements to TPS under various radiotherapy conditions. (d) MCIFF measurement results in 1000 MU and selection of ROI used for dose calculation.

consistent because both FXG film and Cherenkov light spectra are independent of particle energy (6,10 MV and 6,12 MeV) and dose rate (200,400,600 MU/min).[12,24] Such an observation suggests that our proposed technique can be widely applied under all radiation conditions. At a significance level of 0.05, no statistically significant difference is observed in the dose–response, even when the relative positions of the FXG film and the camera varied by 40° in the horizontal direction. This finding signifies that this absolute dose calibration method may be independent of light intensity. The ratio method is widely applied in the field of biology due to its capability to achieve absolute calibration without being influenced by environmental factors. Some researchers have merged this method with Cherenkov luminescence to measure the pH values of tumor microenvironments during radiotherapy.[25] In a previous study, Oraiqat et al. demonstrated the potential of Cherenkov multispectral imaging as a method for measuring pH changes in vitro using phenol red as a contrast agent.[26] The introduction of a few millimeters thick FXG film on the surface of the human body will enhance the dose received by the skin and potentially modify the delivery to the target area. Further research is needed to comprehensively understand the specific impact of incorporating an FXG film into treatment planning. This will facilitate the effective integration of FXG films into the radiotherapy treatment process. In addition, Figure 3a demonstrates that changes in the thickness of the FXG film have a notable effect on the slope of the fitted line because the change in absorbance is directly related to the transmission distance of light through the material. Increased distances exhibit greater absorption changes. Specifically, a thicker FXG film induces more significant alterations in absorbance, yielding larger slopes in fitting results for MCIFF. Meanwhile, an excessively thick FXG film leads to reduced overall Cherenkov luminescence intensity levels, which subsequently reduces the accuracy within imaging results. Moreover, it is observed that the slopes of the fitted lines for films with different thicknesses are remarkably similar after normalizing the thickness. Therefore, our future research endeavors will encompass an investigation into the impact of film thickness on MCIFF measurements, refinement of the film fabrication process, and determination of the optimal thickness.

As illustrated in Figures 4 and 6, differences between the 2D dose distribution obtained from optical measurement, EBT3 film and the gold-standard TPS are mainly concentrated at the radiation field's edge owing to the optical system's point spread function and scattering.[27] Utilizing the initial Cherenkov light image as the intercept for individual pixel fitted lines aims to eliminate the influence of initial Cherenkov light variations across different locations. This allows for a direct correlation between Cherenkov light changes and the dose. While this approach holds promise in mitigating tissue heterogeneity effects, additional experimental validation is necessary. Given a 60 × 60 pixels ROI, MCIFF can accomplish a full-field absolute dose measurement that conforms to the spatial resolution requirements of clinical radiation therapy standards, achieving a resolution of less than 2 mm. During 2D dose verification, the EMCCD camera employed in this experiment is placed flat on a couch—perpendicular to the direction of the gantry and the plane where the FXG film and EBT3 films are positioned. Thus, when the optical profile and dose distribution are analyzed, no additional optical blur caused by the camera's tilt angle is introduced at the profile's edge position. Furthermore, Cherenkov luminescence images can be directly spatially registered with EBT3 film scanning outcomes without necessitating additional transmission transformations.[28]

This study, however, has limitations. The present research is currently at the experimental stage; thus, the obtained results are not optimal. Further in-depth investigations are required before it can advance to the clinical stage. A limitation of this pilot study is that it employs only one type of tissue phantom to simulate the diverse optical properties of human skin surfaces. And dose distribution comparisons are based solely on the relative dose distribution measured on an EBT3 film and absolute dose calculated by TPS, without a secondary method available for comparison of online absolute dose measurements obtained with MCIFF. In future studies, a larger sample of tissue phantoms will be included to validate the potential of MCIFF in correcting tissue heterogeneity. A secondary method will also be utilized to verify the accuracy of absolute dose measurements. Furthermore, although the Cherenkov light is divided into two parts, the random distribution of stray noise generated by secondary particles during radiation therapy affects the entire sensor. Consequently, achieving accurate measurement results becomes challenging when registering and dividing the two-channel images of Cherenkov light. However, employing an intensified camera allows synchronization with the LINAC. This enables the camera's exposure time to be limited to match the LINAC output's duration, effectively reducing the impact of radiation noise. Additionally, implementing additional radiation shielding using lead plates for the camera and adjusting the camera's imaging angle and distance are effective strategies for reducing noise. To enhance the Cherenkov light signal intensity, the use of carbon quantum dots and liquid scintillators can be employed to augment Cherenkov light emission, thus enhancing the signal-to-noise ratio of imaging.[19,29] Alternatively, during the image processing, selecting a larger ROI can also help reduce the impact of noise, but a larger ROI may lead to a decrease in spatial resolution. In sum, deficiencies remain in the exploration of the accuracy of MCIFF under different radiotherapy conditions, and future research will investigate these issues in depth to enhance the dose measurement accuracy.

5 | CONCLUSIONS

In this paper, we propose a novel method called MCIFF, which combines FXG film with multispectral Cherenkov luminescence imaging to achieve absolute 2D dose measurement online. This approach overcomes the challenge of calibrating light intensity accurately with dose. Through conducting dose measurement experiments under various radiation conditions, we have demonstrated that MCIFF can achieve high accuracy in dose measurement ($R^2 > 0.96$) given different beam conditions while enabling full-field dose monitoring at a spatial resolution below 2 mm. This innovative method mitigates the inherent limitations of Cherenkov luminescence in absolute dose measurement, providing new opportunities for optical dose imaging.

ACKNOWLEDGMENTS

This study was supported by the National Natural Science Foundation of China [grant number 12005102, No. 12075120], Jiangsu Planned Projects for Postdoctoral Research Funds [grant number 2021K078A], and the Natural Science Foundation of Jiangsu Province [grant number BK20220132].

CONFLICT OF INTEREST STATEMENT

The authors have no conflicts to disclose.

REFERENCES

1. Chandra RA, Keane FK, Voncken FEM, Thomas CR. Contemporary radiotherapy: present and future. *Lancet*. 2021;398(10295):171-184. doi:10.1016/S0140-6736(21)00233-6
2. Citrin DE. Recent developments in radiotherapy. *N Engl J Med*. 2017;377(11):1065-1075. doi:10.1056/NEJMra1608986
3. Shiau A, Lai P, Liang J, Shueng P, Chen W, Kuan W. Dosimetric verification of surface and superficial doses for head and neck IMRT with different PTV shrinkage margins. *Med Phys*. 2011;38(3):1435-1443. doi:10.1118/1.3553406
4. Zhuang AH, Olch AJ. Validation of OSLD and a treatment planning system for surface dose determination in IMRT treatments. *Med Phys*. 2014;41(8 Part1):081720. doi:10.1118/1.4890795
5. Warkentin B, Steciw S, Rathee S, Fallone BG. Dosimetric IMRT verification with a flat-panel EPID. *Med Phys*. 2003;30(12):3143-3155. doi:10.1118/1.1625440
6. Miao T, Bruza P, Pogue BW, et al. Cherenkov imaging for linac beam shape analysis as a remote electronic quality assessment verification tool. *Med Phys*. 2019;46(2):811-821. doi:10.1002/mp.13303
7. Jarvis LA, Hachadorian RL, Jermyn M, et al. Initial clinical experience of Cherenkov imaging in external beam radiation therapy identifies opportunities to improve treatment delivery. *Int J Radiat Oncol*. 2021;109(5):1627-1637. doi:10.1016/j.ijrobp.2020.11.013
8. Cherenkov PA. Radiation from high-speed particles: visible radiation that is shown to differ from luminescence phenomena has important applications. *Science*. 1960;131(3394):136-142. doi:10.1126/science.131.3394.136
9. Jarvis LA, Zhang R, Gladstone DJ, et al. Cherenkov video imaging allows for the first visualization of radiation therapy in real time. *Int J Radiat Oncol*. 2014;89(3):615-622. doi:10.1016/j.ijrobp.2014.01.046
10. Ai Y, Tang X, Shu D, et al. Measurement of dose in radionuclide therapy by using Cerenkov radiation. *Australas Phys Eng Sci Med*. 2017;40(3):695-705. doi:10.1007/s13246-017-0579-6
11. Shu D, Tang X, Geng C, Gong C, Chen D. Determination of the relationship between dose deposition and Cerenkov photons in homogeneous and heterogeneous phantoms during radiotherapy using Monte Carlo method. *J Radioanal Nucl Chem*. 2016;308(1):187-193. doi:10.1007/s10967-015-4316-x
12. Alexander DA, Nomezine A, Jarvis LA, Gladstone DJ, Pogue BW, Bruza P. Color Cherenkov imaging of clinical radiation therapy. *Light Sci Appl*. 2021;10(1):226. doi:10.1038/s41377-021-00660-0
13. Wickramasinghe VA, Decker SM, Streeter SS, et al. Color-resolved Cherenkov imaging allows for differential signal detection in blood and melanin content. *J Biomed Opt*. 2023;28(03):036005. doi:10.1117/1.JBO.28.3.036005
14. Bero MA, Gilboy WB, Glover PM. Radiochromic gel dosemeter for three-dimensional dosimetry. *Radiat Phys Chem*. 2001;61(3-6):433-435. doi:10.1016/S0969-806X(01)00289-4
15. Jayson GG, Parsons BJ, Swallow AJ. The mechanism of the fricke dosimeter. *Int J Radiat Phys Chem*. 1975;7(2-3):363-370. doi:10.1016/0020-7055(75)90075-3
16. Gambarini G, Veronese I, Bettinelli L, et al. Study of optical absorbance and MR relaxation of Fricke xylenol orange gel dosimeters. *Radiat Meas*. 2017;106:622-627. doi:10.1016/j.radmeas.2017.03.024
17. Black PJ, Velten C, Wang YF, Na YH, Wuu CS. An investigation of clinical treatment field delivery verification using cherenkov imaging: iMRT positioning shifts and field matching. *Med Phys*. 2019;46(1):302-317. doi:10.1002/mp.13250
18. Rabaeh KA, Al-Zawaydaih HHN, Eyadeh MM, Shatnawi MTM. High optical stability of reusable radiochromic polyvinyl alcohol-iodine gel dosimeter for radiotherapy. *Radiat Phys Chem*. 2022;199:110338. doi:10.1016/j.radphyschem.2022.110338
19. Di X, Geng C, Guo C, et al. Enhanced Cherenkov imaging for real-time beam visualization by applying a novel carbon quantum dot sheeting in radiotherapy. *Med Phys*. 2023;50(2):1215-1227. doi:10.1002/mp.16121
20. Zhang R, Andreozzi JM, Gladstone DJ, et al. Cherenkoscopy based patient positioning validation and movement tracking during post-lumpectomy whole breast radiation therapy. *Phys Med Biol*. 2015;60(1):L1-L14. doi:10.1088/0031-9155/60/1/L1
21. Barazzuol L, Coppes RP, Luijk P. Prevention and treatment of radiotherapy-induced side effects. *Mol Oncol*. 2020;14(7):1538-1554. doi:10.1002/1878-0261.12750
22. Hachadorian RL, Bruza P, Jermyn M, et al. Remote dose imaging from Cherenkov light using spatially resolved CT calibration in breast radiotherapy. *Med Phys*. 2022;49(6):4018-4025. doi:10.1002/mp.15614
23. Hachadorian RL, Bruza P, Jermyn M, Gladstone DJ, Pogue BW, Jarvis LA. Imaging radiation dose in breast radiotherapy by X-ray CT calibration of Cherenkov light. *Nat Commun*. 2020;11(1):2298. doi:10.1038/s41467-020-16031-z
24. Moussous O, Khoudri S, Benguerba M. Characterization of a Fricke dosimeter at high energy photon and electron beams used in radiotherapy. *Australas Phys Eng Sci Med*. 2011;34(4):523-528. doi:10.1007/s13246-011-0093-1
25. Czupryna J, Kachur AV, Blankemeyer E, et al. Cerenkov-specific contrast agents for detection of pH in vivo. *J Nucl Med*. 2015;56(3):483-488. doi:10.2967/jnumed.114.146605
26. Oraiqat I, Al-Snayyan E, Calcaterra A, Clarke R, Rehemtulla A, El Naqa I. Measuring tumor microenvironment pH during radiotherapy using a novel Cerenkov emission multispectral optical probe based on silicon photomultipliers. *Front Phys*. 2021;9:636001. doi:10.3389/fphy.2021.636001
27. Bruza P, Lin H, Vinogradov SA, Jarvis LA, Gladstone DJ, Pogue BW. Light sheet luminescence imaging with Cherenkov excitation in thick scattering media. *Opt Lett*. 2016;41(13):2986. doi:10.1364/OL.41.002986

28. Alexander DA, Zhang R, Bruza P, Pogue BW, Gladstone DJ. Scintillation imaging as a high-resolution, remote, versatile 2D detection system for MR-linac quality assurance. *Med Phys*. 2020;47(9):3861-3869. doi:10.1002/mp.14353
29. Tendler I, Bruza P, Andreozzi J, et al. Rapid multisite remote surface dosimetry for total skin electron therapy: scintillator target imaging. *Int J Radiat Oncol*. 2019;103(3):767-774. doi:10.1016/j.ijrobp.2018.10.030

How to cite this article: Han H, Geng C, Deng X, Li J, Shu D, Tang X. A preliminary study of multispectral Cherenkov imaging and a Fricke-xylenol orange gel film (MCIFF) for online, absolute dose measurement. *Med Phys*. 2024;51:3734–3745.
https://doi.org/10.1002/mp.16942